Geology, published online on 21 October 2011 as doi:10.1130/G32073.1

Aseismic sliding of active faults by pressure solution creep: Evidence from the San Andreas Fault Observatory at Depth

J.-P. Gratier[1], J. Richard[1], F. Renard[1,2], S. Mittempergher[3], M.-L. Doan[1], G. Di Toro[3,4], J. Hadizadeh[5], and A.-M. Boullier[1]
[1]ISTerre (Institut des Sciences de la Terre) Observatoire, Université Joseph Fourier Grenoble, CNRS, BP 53, Grenoble 38041, France
[2]Physics of Geological Processes, University of Oslo, 0316 Oslo, Norway
[3]Università di Padova, Via Giotto 1, Padua 35137, Italy
[4]Istituto Nazionale di Geofisica e Vulcanologia, Via di Vigna Murata 605, Rome 00143, Italy
[5]Department of Geography and Geosciences, University of Louisville, Louisville, Kentucky 40292, USA

ABSTRACT

Active faults in the upper crust can either slide steadily by aseismic creep, or abruptly causing earthquakes. Creep relaxes the stress and prevents large earthquakes from occurring. Identifying the mechanisms controlling creep, and their evolution with time and depth, represents a major challenge for predicting the behavior of active faults. Based on microstructural studies of rock samples collected from the San Andreas Fault Observatory at Depth (California), we propose that pressure solution creep, a pervasive deformation mechanism, can account for aseismic creep. Experimental data on minerals such as quartz and calcite are used to demonstrate that such creep mechanism can accommodate the documented 20 mm/yr aseismic displacement rate of the San Andreas fault creeping zone. We show how the interaction between fracturing and sealing controls the pressure solution rate, and discuss how such a stress-driven mass transfer process is localized along some segments of the fault.

INTRODUCTION AND GEOLOGICAL FRAMEWORK

Aseismic deformation is observed in active fault zones, but the mechanisms of deformation are still unclear (Scholz, 2002). Samples collected from the San Andreas Fault Observatory at Depth (SAFOD, California) allow correlation of fault rock microstructures with real-time geophysical data, and therefore provide useful information for identifying such mechanisms. Here we show that a stress-driven mass transfer process, i.e., pressure solution creep (Rutter and Mainprice, 1978), can accommodate the aseismic deformation of the San Andreas fault.

The SAFOD borehole, drilled to 3 km depth, is at the southern part of a 175-km-long creeping section of the San Andreas fault (Fig. 1A). The sliding rate is 28 mm/yr in the central part of the creeping segment, and decreases toward both northern and southern ends (Fig. 1B). The creep rate near the SAFOD site is ~20 mm/yr (Fig. 1B), as measured at the surface within a 20-m-thick fault zone (Titus et al., 2006). Such a narrow creeping zone appears to extend through the entire upper crust, coinciding with a zone of observed microseismicity (Nadeau and Dolenc, 2005). The southernmost part of the creeping section, where the creeping rate gradually falls to zero (Fig. 1B), is a zone of repeating M6 earthquakes, the most recent being the 2004 M6 Parkfield earthquake.

At the SAFOD site, the right-lateral displacement of the San Andreas fault has juxtaposed arkosic sandstones and conglomerates of the Pacific plate against the shale, siltstone, and claystone of the North American plate (Fig. 1C). Microstructural observations of the core samples show evidence of deformation across the damaged zone extending to core-parallel depths of 3150–3410 m (Zoback et al., 2010): shear zones alternate with foliated rocks more or less parallel to the San Andreas fault (Solum et al., 2006). Borehole casing deformation revealed two low-seismic-velocity, actively creeping, zones of foliated rocks (Fig. 1C): a main creeping segment (central deforming zone) at 3300.07–3302.81 m and a secondary creeping segment deforming at lower shear rate (southern deforming zone) at 3191.4–3193 m; both the central and southern deforming zones contain serpentine clasts and highly sheared siltstones (Zoback et al., 2010) without clear displacement discontinuity at their boundaries.

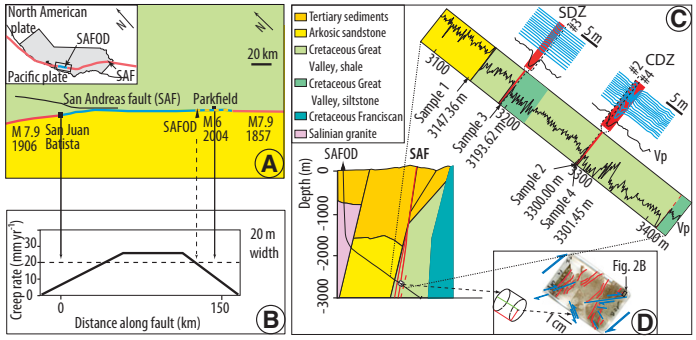

Figure 1. A: Map view of San Andreas fault system showing creeping segment (blue line) with trace of last two M 7.9 earthquakes that currently are locked segments (red lines) and transitional zone of M6 earthquakes (dotted line); coloring corresponds to contact at 3 km depth in C. SAFOD—San Andreas Fault Observatory at Depth. B: Evolution of creep rate along creeping zone (Titus et al., 2006). C: Schematic cross section of SAFOD site, perpendicular to fault; enlargement shows P wave velocity log (Zoback et al., 2010) together with location of four described samples; two creeping faults are highlighted in red; enlargement in vicinity of these creeping zones (top right) shows casing deformation (blue lines) indicating active creep and accurate location of three of the samples. SDZ—southern deforming zone; CDZ—central deforming zone. D: Sketch of thin section (sample 2) perpendicular to foliation (red), with minor faults (blue) (location of Fig. 2B is shown).

EVIDENCE OF PRESSURE SOLUTION CREEP

Based on the microstructural study of samples from the SAFOD core, we infer that an important mechanism of aseismic deformation is pressure solution creep, which induces pervasive and irreversible deformation of the whole rock. This mechanism is active both in the less deformed samples collected from the damaged zone (sample 1) and in intensely deformed foliated samples of the creeping zone (sample 2) shown in Figure 1D. We show that the most highly deformed zones have the highest amount of strain accommodated by pressure solution. Evidence of pressure solution is revealed using elemental distribution maps in sample 1 (Fig. 2A). Stress-driven dissolution associated with horizontal contraction is demonstrated by the dissolution of Ca-Na feldspars at feldspar-quartz grain impingements along a pressure solution seam, whereas K, Mg, Fe, and Ti (phyllosilicates, Fe and Ti oxides, sulfurs) are passively concentrated in the same seam (Fig. 2A). Fracturing is associated with pressure solution. Contraction perpendicular to the dissolution seam, apparent from the grain shape change (Fig. 2A), was estimated to be ~10%. Since there is no evidence of redeposition in veins nearby, it may be concluded that the soluble species have been transported away from the zone of dissolution.

In sample 2, Ca, Si, and Na are depleted within the solution seams where Mg, Fe, Ti are passively concentrated (Fig. 2B). Such a pressure

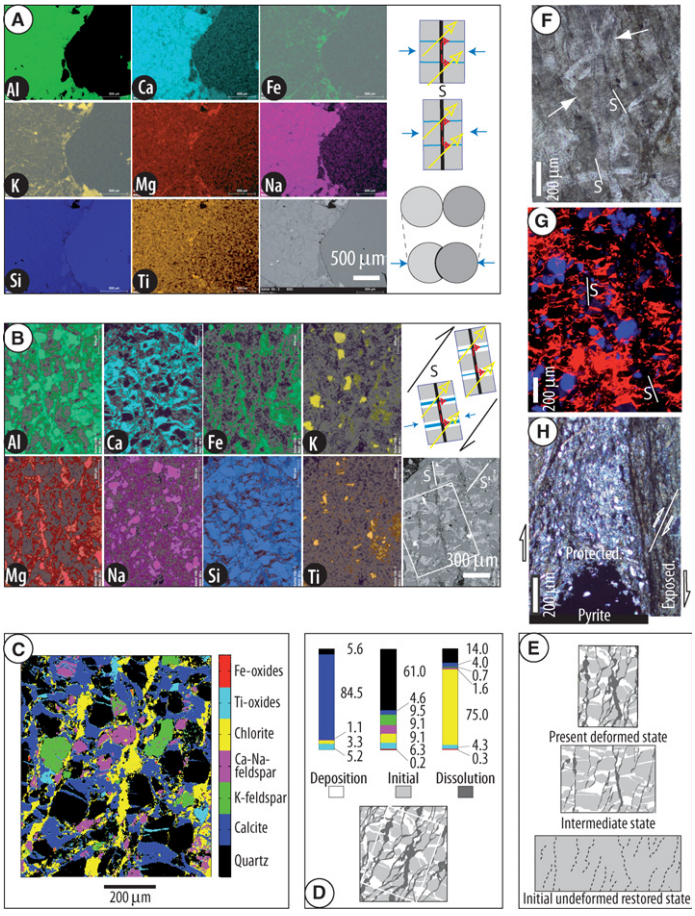

Figure 2. Pressure solution evidence. A and B: Elements distribution from scanning electron microscopy (SEM) analyses for samples 1 and 2, respectively; brighter color indicates higher content; small sketches show diffusive mass transfer path (red arrows) from solution seams (black) (S) to fluid (blue) within vein (white) and fluid flow (yellow). C: Mineralogical distribution in white rectangle area of B (bottom right), sample 2. D: Same area as C. Top—mineral composition of deposition, initial, and dissolution zones. Bottom—areas of three zones are 27%, 58%, and 15%, respectively. E: Present deformed state (top) and restored undeformed state (bottom) of area of white rectangle of D with intermediate deformed state (middle). F: Evidence of stress dissolution of calcite (arrows) within vein with pressure solution seams (S), sample 3. G: Calcite filling of fracture network (orange) perpendicular to solution cleavage (S) (cathodoluminescence, sample 3). H: Stress shadow effect showing evidence of pressure solution grain size reduction from protected to exposed zone with quartz and feldspar depletion, sample 3. (Images A, B, F, G, H can be seen in larger view in the GSA Data Repository[1].)

solution process leads to a foliation oriented at a high angle to the drillhole axis (Figs. 1C and 1D). In contrast to sample 1, calcite minerals in sample 2 fill a network of veins oriented perpendicular to the solution seams, consistent with an extension parallel to the foliation. Finite deformation can be calculated from mineral distribution (Fig. 2C). Three zones are distinguished (Fig. 2D): (1) a dissolution zone (with passively concentrated chlorites and Fe oxides), (2) a deposition zone (with precipitated calcite and occasional Ti oxides), and (3) an initial zone (predeformation zone composed of quartz, feldspars, and chlorites). Veins open and seal progressively (Mittempergher et al., 2011). Consequently, initial zones are dissolved at the beginning of the pressure solution process, then both initial and deposition zones are progressively dissolved (Figs. 2E and 2F). The relative mass change, $\Delta M/M_0$, is calculated using the passive concentration of insoluble minerals in the dissolution zone compared with the composition of the protected zone between solution seams (Figs. 2D and 2E) as:

$$\Delta M / M_0 = \left(I_p / I_d\right) - 1, \quad (1)$$

where I_p and I_d are the content in insoluble minerals in the protected and in the dissolution zone, respectively, and M_0 is the mass of a representative volume element before deformation. Two end members of mass transfer amount are obtained by comparing the composition of dissolution zones with the protected zones: either initial zones or both initial and deposition zones. The two calculations give about the same amounts of relative mass decrease for the dissolution zones (−88% to −90%). A mean value of contraction perpendicular to the foliation of ~60% can be calculated by taking into account the areas of the dissolution zones (Fig. 2D). A mean extension of ~50% perpendicular to the veins is evaluated from the ratio of deposition areas to initial areas (Figs. 2D and 2E). The mass decrease of each soluble mineral that shows no significant differential alteration between protected and dissolution zones can also be calculated (Gratier et al., 2003): quartz, −96%; K-feldspars, −99%; Ca-Na feldspars, −98%; calcite, −94%. Foliation as mineral segregation appears to be linked to the pressure solution creep, with an almost complete disappearance of the soluble minerals in the zones of dissolution. Mass conservation calculations comparing the amounts of dissolved Ca-Na feldspars and deposited minerals in veins show that a large proportion of calcite must come from outside the studied area, brought by episodic fluid flow (Mittempergher et al., 2011). Evidence of dextral shearing is found in thin sections cut normal to the foliation cleavage from both en echelon fractures (Fig. 1D) and crosscutting cleavages (S and S′, Fig. 2B). Consequently, the calcite vein network and the solution cleavage surfaces are consistent with a stress-driven mass transfer process that accommodates right-lateral strike-slip movement along the San Andreas fault (Fig. 2B). Similar solution cleavage–vein network texture (Fig. 3A) is recorded in samples collected near the creeping zone of the southern deforming zone (sample 3, Fig. 2G), but accommodating lower finite strain than in the central deforming zone. Pressure solution creep also develops at grain scale by diffusion-accommodated grain sliding (Fig. 3B; Ashby and Verrall, 1973) within highly sheared and foliated shale in which feldspar and quartz are depleted by the pressure solution process. This can be seen both near the southern deforming zone (sample 3, Fig. 2H) and in the middle of the central deforming zone (sample 4, Fig. 3E). Evidence of dissolution is documented at grain contacts in the SAFOD creeping zones (Schleicher et al., 2009).

KINETICS OF PRESSURE SOLUTION CREEP

A key issue is whether pressure solution kinetics are consistent with the measured permanent fault creep rates (Titus et al., 2006). To solve this issue, we propose a model (Fig. 3) where steady-state creeping occurs within a vertical shear zone as much as 10 km deep. We use a pressure solution creep law for quartz and calcite derived from laboratory indentation experiments (Gratier et al., 2009; Zubtsov et al., 2005). The strain rate $\dot{\varepsilon}$ derived from the experimental relationship is:

$$\dot{\varepsilon} = \Delta d / (d\Delta t) = 8DwcV_s \left(e^{3\Delta\sigma_n V_s/RT} - 1\right) / d^3, \quad (2)$$

where c is the solubility of the diffusing solid, V_s is the molar volume of the stressed solid, R is the gas constant, T is temperature, D is the diffusion constant along the stressed interface, w is the thickness of the trapped fluid phase along which diffusion occurs, t is time, and $\Delta\sigma_n$ is the driving stress as the difference between normal stress on a dissolution surface and the fluid pressure in the vein. In experiments, d is the diam-

[1]GSA Data Repository item 2011336, Figures DR1 and DR2, is available online at www.geosociety.org/pubs/ft2011.htm, or on request from editing@geosociety.org or Documents Secretary, GSA, P.O. Box 9140, Boulder, CO 80301, USA.

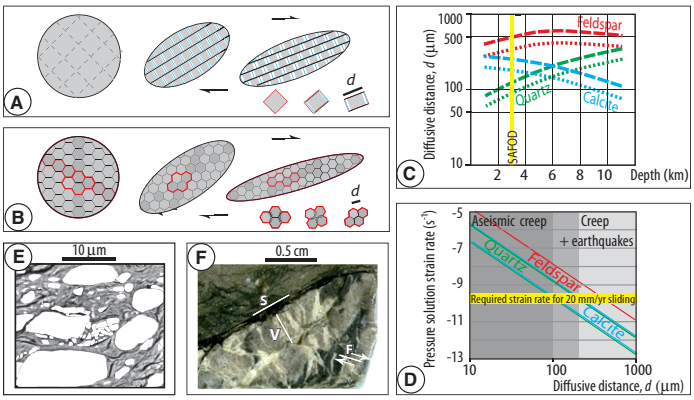

Figure 3. Pressure solution creep mechanisms. A: Mass transfer from solution cleavage (black) to veins (white) with detail of progressive mass transfer process for given element; *d* is mean diffusion distance between veins along solution cleavage; free fluid in veins is blue. B: Diffusion-accommodated grain sliding, with detail of geometry of progressive grain sliding (Ashby and Verrall, 1973); *d* is mean diffusion distance. C: Distance of diffusive mass transfer *d* versus depth for various minerals required to accommodate 20 mm/yr horizontal displacement rate by pressure solution creep in vertical shear zone of 1 m width (dotted line, strain rate of 3.3×10^{-10} s^{-1}) or 3 m width (dashed lines, strain rate of 1.1×10^{-10} s^{-1}). SAFOD—San Andreas Fault Observatory at Depth. D: Pressure solution strain rate versus distance of diffusive mass transfer through entire crust for various minerals; minimum and maximum values for quartz and calcite; yellow line is required strain rate for creeping zone. E: Scanning electron microscope image of sample 4, within creeping zone of central deforming zone (CDZ), showing mixing of phyllosilicates (soft smectite, chlorite, in various grays) and soluble-rigid minerals (quartz, feldspars, calcite, serpentine, in white); crack networks (black) are linked to dewatering of smectite during sample preparation. Deformation is accommodated by grain boundary sliding, possibly by diffusion for soluble species. F: Remnant of sandstone patch deformed by pressure solution cleavage (S)–veins (V) process embedded in CDZ creeping zone, with microfaults (F) (sample 4). (Images E and F can be seen in larger view in the Data Repository [see footnote 1].)

eter of the indenter. In nature, *d* can refer either to the spacing between fractures that corresponds to the diffusive mass transfer distance between veins along a dissolution surface (Fig. 3A), to the grain size in the case of diffusion-accommodating grain boundary sliding (Fig. 3B). Such a diffusion-controlled pressure solution creep law is likely to operate in conditions prevailing at 6–10 km, whereas for the lesser depths (2–4 km), a shift from diffusion control to reaction control is predicted (Renard et al., 1999), but only if *d* exceeds 300 µm, which is not likely here (see following). It is possible to extend the creep law for quartz obtained at 350 °C to lower temperatures within the entire upper crust by assuming an activation energy of 15 kJ/mole (Rutter and Mainprice, 1978). It is also possible to extend the creep law to other minerals such as calcite (Zubtsov et al., 2005) and feldspars by changing the solubility and molar volume parameters. Using such creep laws, with a given stress condition, we can estimate the maximum values of *d* required to accommodate a displacement rate of 20 mm/yr over a 1–3-m-thick shear zone, such as the central deforming zone (Fig. 1C). At 3 km depth, a minimum conservative value for the pressure solution driving stress is the difference between the maximum and the minimum horizontal stress (S_{hmax} and S_{hmin}, respectively). This difference was measured to be ~60 MPa, S_{hmin} being very near the overburden stress (Hickman and Zoback, 2004). The same stress value was used for the entire upper crust (Figs. 3C and 3D). With this model, we show that the maximum required distance of mass transfer at 3 km depth varies with mineral composition in the range 90–350 µm and 125–500 µm for 1 and 3 m width fault zones, respectively (Fig. 3C). These values are larger than the fracture spacing observed for samples 2 and 3 (solution cleavage–veins process; Figs. 2E–2G). They are also much larger than the observed grain sizes in the foliated zones, as in sample 3 and 4 (diffusion-accommodated grain-sliding process; Figs. 2H and 3E). Since the observed diffusion distances are smaller than a conservatively calculated *d* value, pressure solution creep can therefore easily accommodate the measured displacement rate of 20 mm/yr. The diffusion-accommodated grain-sliding process can accommodate much larger finite deformations than the solution cleavage–veins process (Ashby and Verrall, 1973). For this reason, with increasing deformation, the part of the rock deformed by the solution cleavage–veins process, which is also relevant to the most rigid part of the deformed zone, is probably progressively dilacerated and dispersed into the creeping zone (e.g., dark gray grains, Fig. 3B). Evidence of large patches of sandstone deformed by the solution cleavage–veins process can be found in the middle of the central deforming zone (sample 4, Fig. 3F). The solution cleavage–veins process appears therefore to be a transitory state of deformation, which testifies to the efficiency of the pressure solution mechanism and is probably superseded by the diffusion-accommodated grain-sliding process within the most deformed regions of creep.

DISCUSSION AND CONCLUSION

Interaction between creep and seismic (microseismic) fracturing is an important issue. Dissolution indenter experiments show that grain-scale fracturing can drastically accelerate the displacement rate accommodated by pressure solution creep (Gratier, 2011); fracturing opens new paths for solute transport along fluid-filled fractures, decreasing the distance of diffusion, *d*. However, if the fractures are progressively sealed, this effect disappears as sealing increases the distance of mass transfer (*d*), and consequently reduces the displacement rate. At grain scale in the laboratory, such a microfracture pressure solution sealing process may be observed within no less than a few months. In nature, pressure solution fracture sealing probably takes several years or decades, depending on the spacing and the width of the fractures (Gratier, 2011). This could partially explain the effect of the A.D. 2004 M6 Parkfield earthquake on the creep rate southeast of the SAFOD site: coseismic fracturing activated afterslip creep (Freed, 2007) that progressively decreased with time as the fault healed (Li et al., 2006).

The crucial role of the diffusion distance *d* is shown in Figure 3D. When *d* is small enough (10–100 µm), steady-state pressure solution creep can accommodate the observed aseismic displacement rate of 20 mm/yr through the entire upper crust. When *d* is larger (>100 µm), pressure solution creep occurs but cannot accommodate the displacement rate and relax the stress. Consequently, small seismic ruptures occur (Fig. 3F), in turn activating pressure solution creep.

Pressure solution creep is compatible with the low heat flow measurements in the creeping section (Zoback et al., 2010), since this process does not generate significant heat. Various explanations have been proposed for the apparent low friction behavior of the creeping zone. Increases in fluid pressure may reduce the frictional resistance to sliding (Scholz, 2002), but elevated fluid pressures were not measured during drilling, although transient increases of fluid pressure may have occurred episodically in the past (Mittempergher et al., 2011). Talc minerals were found in SAFOD cuttings and should have a weakening effect (Moore and Rymer, 2007), especially if they develop a foliation (Collettini et al., 2009). However, there is as yet no evidence for the presence of continuous layers of talc at SAFOD (Holdsworth et al., 2011). Alternatively, from experiment on cuttings, or laboratory-ground samples, of San Andreas fault creeping zones, Carpenter et al. (2011) and Lockner et al. (2011) found friction values as low as 0.15–0.2, due to the presence of weak phyllosilicate as saponite. It is clear from samples of the San Andreas fault creeping zone (Fig. 3E) that the deformation is accommodated by grain boundary sliding. Friction and

diffusion may compete to accommodate such grain sliding, but it is likely that, at an imposed strain rate, the less energy-consuming process will win. Pressure solution driving forces of 10 and 0.01 MPa are enough to accommodate 10^{-10} s^{-1} strain rate over 3 m width, with 100 and 10 µm grain size, respectively, for quartz and calcite at 6 km depth. Moreover, saponite becomes unstable above ~150 °C and is unlikely to be found deeper in the fault zone than 3.5–4 km. Consequently, as long as the deformation requires grain boundary sliding involving soluble minerals, pressure solution creep is an efficient mechanism of aseismic creep through the entire upper crust down to more than 10 km.

A final question is why, at a given time, pressure solution creep is localized along some segments of the fault. The answer may be that pressure solution creep needs specific conditions to develop at a significant rate. Soluble minerals such as feldspar, calcite, quartz (Gratier et al., 2003), and serpentine (Andreani et al., 2005) must be present with a reactive fluid phase. The distance of diffusive mass transfer (*d*) must be as small as possible. This requires very fine grained material, possibly related to intense seismic fracturing in the San Andreas fault. Soluble grains must not seal together in order to keep fast diffusive paths along solution seams (Niemeijer and Spiers, 2005). Two processes could avoid such sealing, and occur in the San Andreas fault creeping zones, i.e., passive concentration of phyllosilicates due to soluble species pressure solution depletion (Figs. 2H, 3E, and 3F) and the growth of new phyllosilicates (Holdsworth et al., 2011). In such a way, phyllosilicates get trapped around the soluble species, preventing their sealing and activating diffusive mass transfer. Under these conditions, the process is self-organized through a positive feedback process, which allows pressure solution creep process localization within some fault segments.

ACKNOWLEDGMENTS

We thank S. Hickman and B. Holdsworth for their suggestions on an early version, and F. Agosta, C. Colletini, and J. Imber for their comments on the final version that significantly improved the manuscript. The Grenoble team was partially supported by CNRS-INSU (Centre National de la Recherche Scientifique–Institut National des Sciences de l'Univers) natural hazards program and Agence Nationale de la Recherche ANR-09-JCJC-0011-1. Hadizadeh and Di Toro were partially supported by U.S. National Science Foundation grant EAR-0545472. Di Toro and Mittempergher were supported by a Progetti di Eccellenza Fondazione Cassa di Risparmio di Padova e Rovigo and by European Research Council Starting Grant Project 205175.

REFERENCES CITED

Andreani, M., Boullier, A.-M., and Gratier, J.-P., 2005, Development of schistosity by dissolution-crystallization in a Californian serpentinite gouge: Journal of Structural Geology, v. 27, p. 2256–2267, doi:10.1016/j.jsg.2005.08.004.

Ashby, M., and Verrall, R., 1973, Diffusion-accommodated flow and superplasticity: Acta Metallurgica, v. 21, p. 149–163, doi:10.1016/0001-6160(73)90057-6.

Carpenter, B.M., Marone, C., and Saffer, D.M., 2011, Weakness of the San Andrea Fault revealed by samples from the active fault zone: Nature Geoscience, v. 4, p. 251–254, doi:10.1038/ngeo1089.

Collettini, C., Niemeijer, A., Viti, C., and Marone, C., 2009, Fault zone fabric and fault weakness: Nature, v. 462, p. 907–910, doi:10.1038/nature08585.

Freed, A.M., 2007, Afterslip (and only afterslip) following the 2004 Parkfield, California, earthquake: Geophysical Research Letters, v. 34, L06312, doi:10.1029/2006GL029155.

Gratier, J.-P., 2011, Fault permeability and strength evolution related to fracturing and healing episodic processes (years to millennia): The role of pressure solution: Oil & Gas Science and Technology, v. 66, no. 3, doi:10.2516/ogst/2010014.

Gratier, J.-P., Favreau, P., and Renard, F., 2003, Modeling fluid transfer along Californian faults when integrating pressure solution crack sealing and compaction process: Journal of Geophysical Research, v. 108, no. B2, p. 28–52, doi:10.1029/2001JB000380.

Gratier, J.-P., Guiguet, R., Renard, F., Jenatton, L., and Bernard, D., 2009, A pressure solution creep law for quartz from indentation experiments: Journal of Geophysical Research, v. 114, B03403, doi:10.1029/2008JB005652.

Hickman, S., and Zoback, M., 2004, Stress orientations and magnitudes in the SAFOD pilot hole: Geophysical Research Letters, v. 31, L15S12, doi:10.1029/2004GL020043.

Holdsworth, R.E., van Diggelen, E.W.E., Spiers, C.J., de Bresser, J.H.P., Walker, R.J., and Bowen, L., 2011, Fault rocks from the SAFOD core samples: Implications for weakening at shallow depths along the San Andreas fault, California: Journal of Structural Geology, v. 33, p. 132–144, doi:10.1016/j.jsg.2010.11.010.

Li, Y.G., Chen, P., Cochran, E.S., Vidale, J.E., and Burdette, T., 2006, Seismic evidence for rock damage and healing on the San Andreas fault associated with the 2004 M 6.0 Parkfield earthquake: Seismological Society of America Bulletin, v. 96, p. S349–S363, doi:10.1785/0120050803.

Lockner, D.A., Morrow, C., Moore, D.E., and Hickman, S., 2011, Low strength of deep San Andreas fault gouge from SAFOD core: Nature, v. 472, p. 82–85, doi: 101038/Nature09927.

Mittempergher, S., Di Toro, G., Gratier, J.-P., Hadizadeh, J., Smith, S.A.F., and Spiess, R., 2011, Evidence of transient increases of fluid pressure in SAFOD phase III cores: Geophysical Research Letters, v. 38, L03301, doi:10.1029/2010GL046129.

Moore, D.E., and Rymer, M.J., 2007, Talc-bearing serpentinite and the creeping section of the San Andreas fault: Nature, v. 448, p. 795–797, doi:10.1038/nature06064.

Nadeau, R.M., and Dolenc, D., 2005, Nonvolcanic tremors deep beneath the San Andreas Fault: Science, v. 307, p. 389, doi:10.1126/science.1107142.

Niemeijer, A., and Spiers, C.-J., 2005, Influence of phyllosilicates on fault strength in the brittle-ductile transition: Insight from rock analogue experiments, *in* Bruhn, D., and Burlini, L., eds., High-strain zones: Structure and physical properties: Geological Society of London Special Publication 245, p. 303–327, doi:10.1144/GSL.SP.2005.245.01.15.

Renard, F., Park, A., Ortoleva, P., and Gratier, J.-P., 1999, An integrated model for transitional pressure solution in sandstones: Tectonophysics, v. 312, p. 97–115, doi:10.1016/S0040-1951(99)00202-4.

Rutter, E.H., and Mainprice, D.H., 1978, The effect of water on stress relaxation of faulted and unfaulted sandstones: Pure and Applied Geophysics, v. 116, p. 634–654, doi:10.1007/BF00876530.

Schleicher, A.M., Tourscher, S.N., van der Pluijm, B.A., and Warr, L.N., 2009, Constraints on mineralization, fluid-rock interaction, and mass transfer during faulting at 2–3 km depth from the SAFOD drill hole: Journal of Geophysical Research, v. 114, B04202, doi:10.1029/2008JB006092.

Scholz, C., 2002, The mechanics of earthquakes and faulting: Cambridge, Cambridge University Press, 439 p.

Solum, J.G., Hickman, S.H., Lockner, D.A., Moore, D.E., van der Pluijm, B.A., Schleicher, A.M., and Evans, J.P., 2006, Mineralogical characterization of protolith and fault rocks from the SAFOD Main Hole: Geophysical Research Letters, v. 33, L21314, doi:10.1029/2006GL027285.

Titus, S.J., DeMets, C., and Tikoff, B., 2006, Thirty-five-year creep rates for the creeping segment of the San Andreas fault and the effects of the 2004 Parkfield earthquake: Constraints from alignment arrays, continuous global positioning system, and creepmeters: Seismological Society of America Bulletin, v. 96, p. S250–S268, doi:10.1785/0120050811.

Zoback, M., Hickman, S., and Ellsworth, W., 2010, Scientific drilling into the San Andreas fault zone: Eos (Transactions, American Geophysical Union), v. 91, p. 197–199, doi:10.1029/2010EO220001.

Zubtsov, S., Renard, F., Gratier, J.-P., Dysthe, D.K., and Traskine, V., 2005, Single-contact pressure solution creep on calcite monocrystals, *in* Gapais, D., et al., eds., Deformation mechanisms, rheology and tectonics: From minerals to the lithosphere: Geological Society of London Special Publication 243, p. 81–95, doi:10.1144/GSL.SP.2005.243.01.08.

Manuscript received 14 January 2011
Revised manuscript received 31 May 2011
Manuscript accepted 9 July 2011

Printed in USA